Comput Mech (2005) 36: 62–75
DOI 10.1007/s00466-004-0642-5

ORIGINAL PAPER

S. Rahman · B. N. Rao

Continuum Shape Sensitivity analysis of a mode-I fracture in functionally graded materials

Received: 22 July 2004 / Accepted: 28 October 2004/ Published online: 17 December 2004

Abstract This paper presents a new method for conducting a continuum shape sensitivity analysis of a crack in an isotropic, linear-elastic, functionally graded material. This method involves the material derivative concept from continuum mechanics, domain integral representation of the *J*-integral and direct differentiation. Unlike virtual crack extension techniques, no mesh perturbation is needed to calculate the sensitivity of stress-intensity factors. Since the governing variational equation is differentiated prior to the process of discretization, the resulting sensitivity equations are independent of approximate numerical techniques, such as the meshless method, finite element method, boundary element method, or others. In addition, since the *J*-integral is represented by domain integration, only the first-order sensitivity of the displacement field is needed. Several numerical examples are presented to calculate the first-order derivative of the *J*-integral, using the proposed method. Numerical results obtained using the proposed method are compared with the reference solutions obtained from finite-difference methods for the structural and crack geometries considered in this study.

Keywords Crack · Functionally graded materials · *J*-integral · Linear-elastic fracture mechanics · Shape sensitivity analysis · Material derivative

S. Rahman
Department of Mechanical and Industrial Engineering, The University of Iowa, Iowa City, IA 52242, USA
E-mail: rahman@engineering.uiowa.edu
Tel.: +1-319-335-5679
Fax: +1-319-335-5669

B. N. Rao (✉)
Structural Engineering Division, Department of Civil Engineering, Indian Institute of Technology, Madras, Chennai, PIN 600 036, India
E-mail: bnrao@iitm.ac.in
Tel.: 91-44-22578498
Fax: 91-44-22578327

1. Introduction

In recent years, functionally graded materials (FGMs) have been introduced and applied in the development of structural components subject to non-uniform service requirements. FGMs, which possess continuously varying microstructural, mechanical and/or thermal properties, are essentially two-phase particulate composites, such as ceramic and metal alloy phases, synthesized such that the composition of each constituent changes continuously in one direction to yield a predetermined composition profile [1]. The absence of sharp interfaces in FGM greatly reduces material property mismatch, which has been found to improve resistance to interfacial delamination and fatigue crack propagation [2]. However, because the microstructure of FGM is generally heterogeneous, its dominant type of failure is crack initiation and growth from inclusions. The extent to which constituent material properties and the microstructure can be tailored to guard against potential fracture and failure patterns is relatively unknown. Such issues have motivated much of the current research into the numerical computation of stress intensity factors (SIFs) and its impact on the fracture of FGMs [3, 4]. However, in many applications of fracture mechanics, derivatives of SIF with respect to crack size are also needed for predicting stability and the arrest of crack propagation in FGM. Another major use of SIF derivatives is in the reliability analysis of cracked structures. For example, first- and second-order reliability methods [5] frequently used in probabilistic fracture mechanics [6–12] require the gradient and Hessian of the performance function with respect to crack length. In a linear-elastic fracture, the performance function builds on SIF. Hence, both first and second-order derivatives of SIF are needed for probabilistic analysis.

For predicting the sensitivities of SIF under a mode-I condition, some methods have already appeared for homogenous materials. In 1988, Lin and Abel [13] employed a virtual crack extension technique [14–17]

and the variational formulation in conjunction with the finite element method (FEM) to calculate the first-order derivative of SIF for a structure containing a single crack. Subsequently, Hwang et al. [18] generalized this method to calculate both first and second-order derivatives for structures involving multiple crack systems, an axisymmetric stress state, and crack-face and thermal loading. However, these methods require mesh perturbation, which is a fundamental requirement of all virtual crack extension techniques. For second-order derivatives, the number of elements surrounding the crack tip affected by mesh perturbation has a significant effect on solution accuracy. To overcome this problem, Chen et al. [19–21] recently applied concepts from shape sensitivity analysis to calculate the first-order derivative of SIFs. In this new method, the domain integral representation of the *J*-integral (mode-I) or the interaction integral (mixed-mode) is invoked and the material derivative concept from continuum mechanics is then used to obtain the first-order sensitivity of SIFs. However, the sensitivity equations presently available are valid only for analyzing cracks in homogenous materials. Hence, there is a clear need to develop new sensitivity equations for cracks in FGMs.

This paper presents a new method for conducting continuum shape sensitivity analyses of a mode-I crack in an isotropic, linear-elastic FGM. The method involves the material derivative concept from continuum mechanics, domain integral representation of a *J*-integral, and direct differentiation. This paper is organized as follows. Section 2 presents continuum shape sensitivity analysis for non-homogeneous materials. Section 3 explains the *J*-integral and the sensitivity of *J*-integral formulation for FGMs. This section also illustrates the velocity field that was adopted in this study. Section 4 presents several numerical examples to demonstrate the performance of the proposed continuum shape sensitivity analysis method for non-homogeneous materials. Finally, Section 5 presents summaries and conclusions concerning the proposed formulation. Numerical results of first-order sensitivities of *J*-integral or stress intensity factors obtained using the proposed method are compared with the reference solutions obtained using the finite-difference method.

2. Shape sensitivity analysis

2.1 Velocity field

Consider a general three-dimensional body with a specific configuration, referred to as the reference configuration, with domain Ω, boundary Γ, and a body material point identified by position vector $\boldsymbol{x} \in \Omega$. Consider the motion of the body from the configuration with domain Ω and boundary Γ into another configuration with domain Ω_τ and boundary Γ_τ, as shown in Fig. 1. This process can be expressed as

$$\boldsymbol{T}: \boldsymbol{x} \to \boldsymbol{x}_\tau, \boldsymbol{x} \in \Omega \tag{1}$$

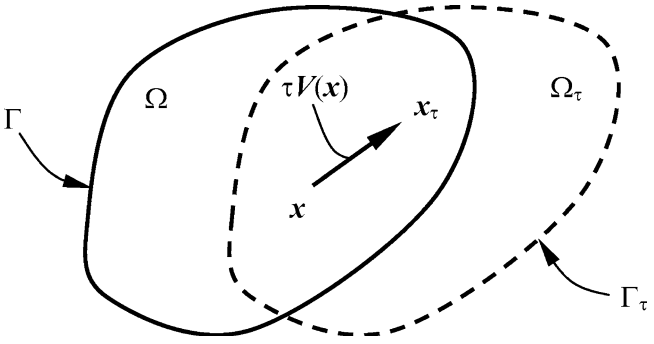

Fig. 1 Variation of domain

where $\boldsymbol{x}$ and $\boldsymbol{x}_\tau$ are the position vectors of a material point in the reference and perturbed configurations, respectively, $\boldsymbol{T}$ is a transformation mapping, and τ is a scalar time-like parameter denoting the amount of shape change with

$$\begin{aligned} \boldsymbol{x}_\tau &= \boldsymbol{T}(\boldsymbol{x}, \tau) \\ \Omega_\tau &= \boldsymbol{T}(\Omega, \tau) \\ \Gamma_\tau &= \boldsymbol{T}(\Gamma, \tau) \end{aligned} \tag{2}$$

A velocity field $\boldsymbol{V}$ can then be defined as

$$\boldsymbol{V}(\boldsymbol{x}_\tau, \tau) = \frac{\mathrm{d}\boldsymbol{x}_\tau}{\mathrm{d}\tau} = \frac{\mathrm{d}\boldsymbol{T}(\boldsymbol{x}, \tau)}{\mathrm{d}\tau} = \frac{\partial \boldsymbol{T}(\boldsymbol{x}, \tau)}{\partial \tau}. \tag{3}$$

In the neighborhood of an initial time $\tau = 0$, assuming a regularity hypothesis and ignoring high-order terms, $\boldsymbol{T}$ can be approximated by

$$\begin{aligned} \boldsymbol{T}(\boldsymbol{x}, \tau) &= \boldsymbol{T}(\boldsymbol{x}, 0) + \tau \frac{\partial \boldsymbol{T}(\boldsymbol{x}, 0)}{\partial \tau} \\ &\quad + O(\tau^2) \cong \boldsymbol{x} + \tau \boldsymbol{V}(\boldsymbol{x}, 0), \end{aligned} \tag{4}$$

where $\boldsymbol{x} = \boldsymbol{T}(\boldsymbol{x}, 0)$ and $\boldsymbol{V}(\boldsymbol{x}) = \boldsymbol{V}(\boldsymbol{x}, 0)$.

2.2 Sensitivity Analysis

The variational governing equation for a non-homogeneous or homogeneous structural component with domain Ω can be formulated as [22, 23]

$$\begin{aligned} a_\Omega(\boldsymbol{z}, \bar{\boldsymbol{z}}) \equiv \int \sigma_{ij}(\boldsymbol{z}) \varepsilon_{ij}(\bar{\boldsymbol{z}}) d\Omega = \ell_\Omega(\bar{\boldsymbol{z}}) \equiv \int_\Omega f_i^b \bar{z}_i \mathrm{d}\Omega \\ + \int_\Gamma T_i \bar{z}_i d\Gamma, \quad \text{for all } \bar{\boldsymbol{z}} \in \boldsymbol{Z} \end{aligned} \tag{5}$$

where $\sigma_{ij}(\boldsymbol{z})$ and $\varepsilon_{ij}(\bar{\boldsymbol{z}})$ are components of the stress and strain tensors of the displacement z and virtual displacement $\bar{\boldsymbol{z}}$, respectively, f_i^b and T_i are the ith component of body force and surface traction, respectively, and $\bar{z}_i$ is the ith component of $\bar{\boldsymbol{z}}$, $\boldsymbol{Z}$ is the space of kinematically admissible virtual displacements, and $a_\Omega(\boldsymbol{z}, \bar{\boldsymbol{z}})$ and $\ell_\Omega(\bar{\boldsymbol{z}})$ are energy bilinear and load linear forms, respectively. The subscript Ω in Eq. (5) is used to indicate the dependency of the governing equation on the shape of the structural domain.

The pointwise material derivative at $\boldsymbol{x} \in \Omega$ is defined as [22, 23]

$$\dot{\boldsymbol{z}} = \lim_{\tau \to 0} \left[\frac{\boldsymbol{z}_\tau(\boldsymbol{x} + \tau \boldsymbol{V}(\boldsymbol{x})) - \boldsymbol{z}(\boldsymbol{x})}{\tau} \right]. \tag{6}$$

If $\boldsymbol{z}_\tau$ has a regular extension to a neighborhood of Ω_τ, then

$$\dot{\boldsymbol{z}}(\boldsymbol{x}) = \boldsymbol{z}'(\boldsymbol{x}) + \nabla \boldsymbol{z}^{\boldsymbol{T}} \boldsymbol{V}(\boldsymbol{x}), \tag{7}$$

where

$$\boldsymbol{z}' = \lim_{\tau \to 0} \left[\frac{\boldsymbol{z}_\tau(\boldsymbol{x}) - \boldsymbol{z}(\boldsymbol{x})}{\tau} \right] \tag{8}$$

is the partial derivative of $\boldsymbol{z}$ and $\tilde{\mathbf{N}} = \{\partial/\partial x_1, \partial/\partial x_2, \partial/\partial x_3\}^T$ is the vector of gradient operators. One attractive feature of the partial derivative is that, given the smoothness assumption, it commutes with the derivatives with respect to x_i, $i = 1, 2,$ and 3, since they are derivatives with respect to independent variables, i.e.,

$$\left(\frac{\partial \boldsymbol{z}}{\partial x_i} \right)' = \frac{\partial}{\partial x_i}(\boldsymbol{z}'), i = 1, 2, \text{ and } 3 \ . \tag{9}$$

Let ψ_1 be a domain functional, defined as an integral over Ω_τ, i.e.,

$$\psi_1 = \int_{\Omega_\tau} f_\tau(\boldsymbol{x}_\tau) \mathrm{d}\Omega_\tau, \tag{10}$$

where f_τ is a regular function defined on Ω_τ. If Ω is C^k regular, then the material derivative of ψ_1 at Ω is [22, 23]

$$\dot{\psi}_1 = \int_\Omega [f'(\boldsymbol{x}) + \mathrm{div} f(\boldsymbol{x}) \boldsymbol{V}(\boldsymbol{x})] \mathrm{d}\Omega. \tag{11}$$

For a functional form of

$$\psi_2 = \int_{\Omega_\tau} g(\boldsymbol{z}_\tau, \boldsymbol{z}_\tau) \mathrm{d}\Omega_\tau \ , \tag{12}$$

the material derivative of ψ_2 at Ω using Eqs. (10) and (12) is [23]

$$\dot{\psi}_2 = \int_\Omega \Big[g_{,z_i} \dot{\boldsymbol{z}}_i - g_{,z_i}(\boldsymbol{z}_{i,j} V_j) + g_{,z_{ij}} \dot{\boldsymbol{z}}_{i,j} - g_{,z_{i,j}}(\boldsymbol{z}_{i,jk} V_k) + \mathrm{div}(g \boldsymbol{V}) \Big] \mathrm{d}\Omega, \tag{13}$$

in which a comma is used to denote partial differentiation, e.g., $z_{i,j} = \partial z_i / \partial x_j$, $z_{i,jk} = \partial^2 z_i / \partial x_j \partial x_k$, $\dot{z}_{i,j} = \partial \dot{z}_i / \partial x_j$, $g_{,z_i} = \partial g / \partial z_i$, $g_{,z_{i,j}} = \partial g / \partial z_{i,j}$ and V_j is the jth component of $\boldsymbol{V}$. In Eq. (13), the material derivative $\dot{\boldsymbol{z}}$ is the solution to the sensitivity equation obtained by taking the material derivative of Eq. (5).

If no body force is involved, the variational equation (Eq. 5) can be written as

$$a_\Omega(\boldsymbol{z}, \bar{\boldsymbol{z}}) \equiv \int_\Omega \sigma_{ij}(\boldsymbol{z}) \varepsilon_{ij}(\bar{\boldsymbol{z}}) \mathrm{d}\Omega = l_\Omega(\bar{\boldsymbol{z}}) \equiv \int_\Gamma T_i \bar{z}_i \mathrm{d}\Gamma, \tag{14}$$

Taking the material derivative of both sides of Eq. (14) and using Eq. (9),

$$a_\Omega(\dot{\boldsymbol{z}}, \bar{\boldsymbol{z}}) = \ell'_{\boldsymbol{V}}(\bar{\boldsymbol{z}}) - a'_{\boldsymbol{V}}(\boldsymbol{z}, \bar{\boldsymbol{z}}), \forall \bar{\boldsymbol{z}} \in \boldsymbol{Z} \tag{15}$$

where subscript $\boldsymbol{V}$ indicates the dependency of the terms on the velocity field. The terms $\ell'_{\boldsymbol{V}}(\bar{\boldsymbol{z}})$ and $a'_{\boldsymbol{V}}(\boldsymbol{z}, \bar{\boldsymbol{z}})$ can be further derived as [22, 23]

$$l'_{\boldsymbol{V}}(\bar{\boldsymbol{z}}) = \int_\Gamma \Big\{ -T_i(\bar{z}_{i,j} V_j) + (T_i \bar{z}_i)_{,j} n_j + \kappa_\Gamma (T_i \bar{z}_i)](V_i n_i) \Big\} \mathrm{d}\Gamma \tag{16}$$

and

$$a'_V(\boldsymbol{z}, \bar{\boldsymbol{z}}) = -\int_\Omega \times \begin{bmatrix} \sigma_{ij}(\boldsymbol{z})(\bar{z}_{i,k} V_{k,j}) + \sigma_{ij}(\bar{\boldsymbol{z}})(\boldsymbol{z}_{i,k} V_{k,j}) - \\ \varepsilon_{ij}(\bar{\boldsymbol{z}}) D_{ijkl,m} \varepsilon_{kl}(\boldsymbol{z}) V_m - \sigma_{ij}(\boldsymbol{z}) \varepsilon_{ij}(\bar{\boldsymbol{z}}) \mathrm{div} \boldsymbol{V} \end{bmatrix} \mathrm{d}\Omega \ , \tag{17}$$

where n_i is the ith component of unit normal vector $\boldsymbol{n}$, κ_Γ is the curvature of the boundary, $z_{i,j} = \partial z_i / \partial x_j$, $\bar{z}_{i,j} = \partial \bar{z}_i / \partial x_j$, $V_{i,j} = \partial V_i / \partial x_j$, D_{ijkl} is the constitutive tensor, and $D_{ijkl,m} = \partial D_{ijkl} / \partial x_m$. Note that the third term in the integrand on the right hand side of Eq. (17) arises

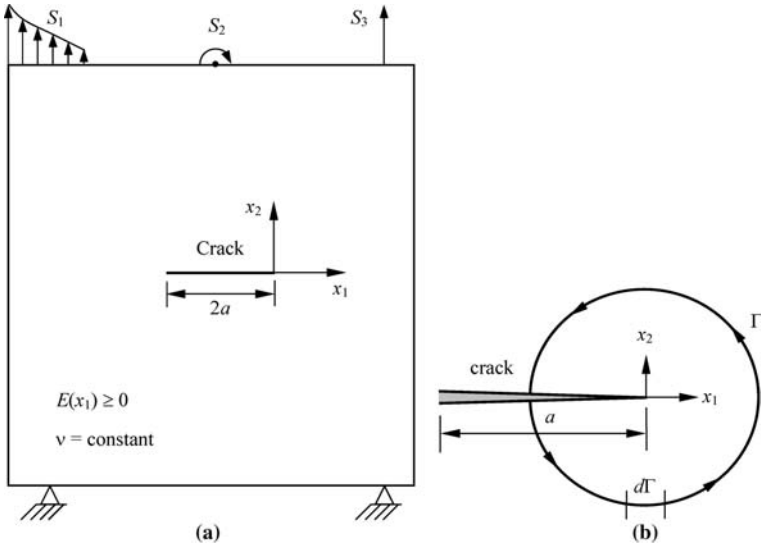

Fig. 2 *J*-integral fracture parameter; **a** A mode-I crack in functionally graded material; and **b** Arbitrary contour around a crack

naturally in the formulation of continuum shape sensitivity analysis for non-homogeneous materials, but vanishes for homogeneous materials. If the modulus of elasticity $E(\boldsymbol{x})$ is the only material property that varies, then $D_{ijkl,m} = (\partial E(\boldsymbol{x})/\partial x_m) D_{ijkl}/E(\boldsymbol{x})$.

To evaluate the sensitivity expression of Eq. (13), a numerical method is needed to solve Eq. (14), for which a standard FEM was used in this study. If the solution $\boldsymbol{z}$ of Eq. (14) is obtained using an FEM code, the same code can be used to solve Eq. (15) for $\dot{\boldsymbol{z}}$. This solution of $\dot{\boldsymbol{z}}$ can be obtained efficiently since it only requires the evaluation of the same set of FEM matrix equations with a different fictitious load, which is the right hand side of Eq. (15).

3. The *J*-integral and its sensitivity

3.1 The *J*-integral

Consider a two-dimensional, linear-elastic, isotropic FGM with a rectilinear crack of length $2a$, subjected to external loads $S_1, S_2, \ldots, S_M$, as shown in Fig. 2(a). It is assumed that the modulus of elasticity E is the only material property that varies, according to

$$E = E(x_1) \geq 0 \tag{18}$$

and is a continuous, bounded, and at least piecewise differentiable function on domain Ω. The x_1–x_2 coordinate system is defined in Fig. 2(a). In reality, FGMs are multi-phase materials with general, locally discontinuous material properties. Hence, $E(x_1)$ in Eq. (18) should be viewed as a smoothly varying "effective" material property of FGM. Also, Poisson's ratio v was held constant. This is a reasonable assumption, since variation of Poisson's ratio is usually small compared with that of the elastic modulus.

Using an arbitrary counter-clockwise path Γ around the crack tip, as shown in Fig. 2(b), the path independent *J*-integral under mode-I condition for a cracked body is given by [24]

$$J = \int_\Gamma \left(W\delta_{1j} - \sigma_{ij}\frac{\partial z_i}{\partial x_i} \right) n_j \mathrm{d}\Gamma, \tag{19}$$

where $W = \int \sigma_{ij} d\varepsilon_{ij}$ is the strain energy density, and n_j is the jth component of the outward unit vector normal to an arbitrary contour Γ enclosing the crack tip. For linear elastic material models it can shown that $W = \sigma_{ij}\varepsilon_{ij}/2 = \varepsilon_{ij} D_{ijkl} \varepsilon_{kl}/2$. Applying the divergence theorem, equilibrium and strain-displacement conditions the contour integral in Eq. (19) can be converted into equivalent domain forms, given by [4]

$$J = \int_A \left(\sigma_{ij}\frac{\partial z_i}{\partial x_i} - W\delta_{1j} \right) \frac{\partial q}{\partial x_j} \mathrm{d}A \tag{20}$$

and

$$J = \int_A \left(\sigma_{ij}\frac{\partial z_i}{\partial x_i} - W\delta_{1j} \right) \frac{\partial q}{\partial x_j} \mathrm{d}A - \int_A \tfrac{1}{2}\varepsilon_{ij}\tfrac{\partial D_{ijkl}}{\partial x_1} q \mathrm{d}A \tag{21}$$

for homogeneous and functionally graded materials, respectively, where δ_{1j} is the Kronecker delta, A is the area inside the contour and q is a weight function chosen such that it has a value of *unity* at the crack tip, *zero* along the boundary of the domain, and is arbitrary elsewhere. By comparing Eq. (21) to the classical *J*-integral in Eq. (20), the presence of material non-homogeneity results in the addition of a second domain integral. Although this integral is negligible for a path very close to the crack tip, it must be accounted for with relatively large integral domains for the *J*-integral to be accurately calculated. The sensitivity formulation presented in the following section as well as all numerical results in the subsequent section are based on the *J*-integral for FGM from Eq. (21).

3.2 Sensitivity of the *J*-integral

For two-dimensional plane stress or plane strain problems, once the stress-strain and strain-displacement relationships are applied, Eq. (21) can be expressed as

$$\begin{aligned} J = & \int_A \left(\sigma_{11}\varepsilon_{11} + \sigma_{12}\frac{\partial z_2}{\partial x_1} \right) \frac{\partial q}{\partial x_1} \mathrm{d}A \\ & + \int_A \left(\sigma_{12}\varepsilon_{11} + \sigma_{22}\frac{\partial z_2}{\partial x_1} \right) \frac{\partial q}{\partial x_2} \mathrm{d}A + \\ & - \left(\tfrac{1}{2}\sigma_{11}\varepsilon_{11} + \sigma_{12}\varepsilon_{12} + \tfrac{1}{2}\sigma_{22}\varepsilon_{22} \right) \frac{\partial q}{\partial x_1} \mathrm{d}A \\ & - \int_A \left(\tfrac{1}{2}\sigma_{11}\varepsilon_{11} q + \sigma_{12}\varepsilon_{12} q + \tfrac{1}{2}\sigma_{22}\varepsilon_{22} q \right) \frac{\partial E}{\partial x_1} \mathrm{d}A, \end{aligned} \tag{22}$$

which can be further simplified as

$$J = \int_A h \mathrm{d}A, \tag{23}$$

where

$$h = h_1 + h_2 + h_3 + h_4 - h_5 - h_6 - h_7 - h_8 - h_9 - h_{10}. \tag{24}$$

with h_i, $i = 1,\ldots, 10$ for those that depend on $\varepsilon_{ij}, z_i, q, E(x_1), v$, and some of their derivatives. The explicit expressions of h, $i = 1,\ldots,10$ are given in Appendix A for both plane stress and plane strain conditions. In accordance with Eq. (11), the material derivative of the *J*-integral can be expressed as

$$\dot{J} = -\int_A [h' + \mathrm{div}(h\boldsymbol{V})] \mathrm{d}A \ , \tag{25}$$

where

$$h' = h'_1 + h'_2 + h'_3 + h'_4 - h'_5 - h'_6 - h'_7 - h'_8 - h'_9 - h'_{10} \tag{26}$$

and $\boldsymbol{V} = \{V_1, V_2\}^T$. Assuming crack length a to be the variable of interest, a change in crack length in the x_1 direction (mode-I) only, i.e., $\boldsymbol{V} = \{V_1, 0\}^T$, results in the expression of Eq. (25) as

$$\dot{J} = \int_A (H_1 + H_2 + H_3 + H_4 - H_5 - H_6 - H_7 - H_8 - H_9 - H_{10})\mathrm{d}A, \quad (27)$$

where

$$H_i = h_i' + \frac{\partial(h_i V_1)}{\partial x_1}, \quad i = 1, \ldots, 10. \quad (28)$$

For illustrative purposes, consider the first term

$$H_1 = h_1' + \frac{\partial(h_1 V_1)}{\partial x_1} \quad (29)$$

under plane stress conditions, which can be expanded as

$$\begin{aligned} H_1 &= \frac{1}{2(1-\nu^2)}\left[\left(E\varepsilon_{11}^2\frac{\partial q}{\partial x_1}\right)' + \frac{\partial}{\partial x_1}\left(E\varepsilon_{11}^2\frac{\partial q}{\partial x_1}V_1\right)\right] \\ &= \frac{E'\varepsilon_{11}^2}{2(1-\nu^2)}\frac{\partial q}{\partial x_1} + \frac{E\varepsilon_{11}\varepsilon_{11}'}{(1-\nu^2)}\frac{\partial q}{\partial x_1} \\ &\quad + \frac{E\varepsilon_{11}^2}{2(1-\nu^2)}\frac{\partial q'}{\partial x_1} + \frac{\varepsilon_{11}^2 V_1}{2(1-\nu^2)}\frac{\partial E}{\partial x_1}\frac{\partial q}{\partial x_1} \\ &\quad + \frac{E\varepsilon_{11}V_1}{(1-\nu^2)}\frac{\partial \varepsilon_{11}}{\partial x_1}\frac{\partial q}{\partial x_1} + \frac{E\varepsilon_{11}^2 V_1}{2(1-\nu^2)}\frac{\partial^2 q}{\partial x_1^2} \\ &\quad + \frac{E\varepsilon_{11}^2}{2(1-\nu^2)}\frac{\partial q}{\partial x_1}\frac{\partial V_1}{\partial x_1}. \end{aligned} \quad (30)$$

In this study, velocity field $\boldsymbol{V}$ was chosen such that the finite element mesh in the domain over which the J-integral in the Eq. (21) is evaluated has a virtual rigid body translation along with the crack tip. Velocity field $\boldsymbol{V}$ is constant in the region over which the J-integral is evaluated, varies smoothly in the rest of the domain, is zero along the boundary excluding the crack face and the essential boundary, and varies smoothly along the crack face and the essential boundary. The velocity field will be explained in more detail in a forthcoming section. Since q is defined around the crack tip in the domain over which the J-integral is evaluated, if the crack tip moves, the value of q around the new crack tip will be same as that of the old crack tip. Hence, $\dot{q} = 0$. Therefore,

$$\begin{aligned} q' &= \dot{q} - \nabla \boldsymbol{V}^T q \boldsymbol{V} = -\nabla^T q \boldsymbol{V} \\ &= -\frac{\partial q}{\partial x_1}V_1 - \frac{\partial q}{\partial x_2}V_2 = -\frac{\partial q}{\partial x_1}V_1 \ . \end{aligned} \quad (31)$$

Also, since velocity field $\boldsymbol{V}$ is constant in the region over which the J-integral is evaluated,

$$\frac{\partial V_i}{\partial x_j} = 0; i, j = 1, 2, \quad (32)$$

which yields

$$\frac{\partial q'}{\partial x_1} = -\frac{\partial^2 q}{\partial x_1^2}V_1 \quad (33)$$

$$\frac{\partial q'}{\partial x_2} = -\frac{\partial^2 q}{\partial x_1 \partial x_2}V_1. \quad (34)$$

Since $E(\boldsymbol{x})$ is independent of the change in crack length,

$$E' = 0. \quad (35)$$

Hence,

$$\dot{E} = \nabla^T E \boldsymbol{V} = \frac{\partial E}{\partial x_1}V_1. \quad (36)$$

Using Eq. (7), and the strain-displacement relationship, it can be shown that

$$\varepsilon_{11}' = \frac{\partial \dot{z}_1}{\partial x_1} - \frac{\partial^2 z_1}{\partial x_1^2}V_1, \quad (37)$$

$$\varepsilon_{22}' = \frac{\partial \dot{z}_2}{\partial x_2} - \frac{\partial^2 z_2}{\partial x_2 \partial x_1}V_1, \quad (38)$$

and

$$\varepsilon_{12}' = \frac{1}{2}\left(\frac{\partial \dot{z}_1}{\partial x_2} - \frac{\partial^2 z_1}{\partial x_2 \partial x_1}V_1 + \frac{\partial \dot{z}_2}{\partial x_1} - \frac{\partial^2 z_2}{\partial x_1^2}V_1\right). \quad (39)$$

Substituting Eqs. (32, 33, 35) and (37) into Eq. (30) followed by simplification leads to

$$H_1 = \frac{E\varepsilon_{11}}{(1-\nu^2)}\frac{\partial \dot{z}_1}{\partial x_1}\frac{\partial q}{\partial x_1} + \frac{\varepsilon_{11}^2 V_1}{2(1-\nu^2)}\frac{\partial E}{\partial x_1}\frac{\partial q}{\partial x_1}. \quad (40)$$

A similar procedure can be carried out using Eq. (31–39) to obtain the remaining expressions of H_i, i = 1,..., 10 for plane stress and plane strain conditions, respectively. Equations B1–B10 and B11–B20 in Appendix B provide explicit expressions of H_i, i = 1,..., 10 for plane stress

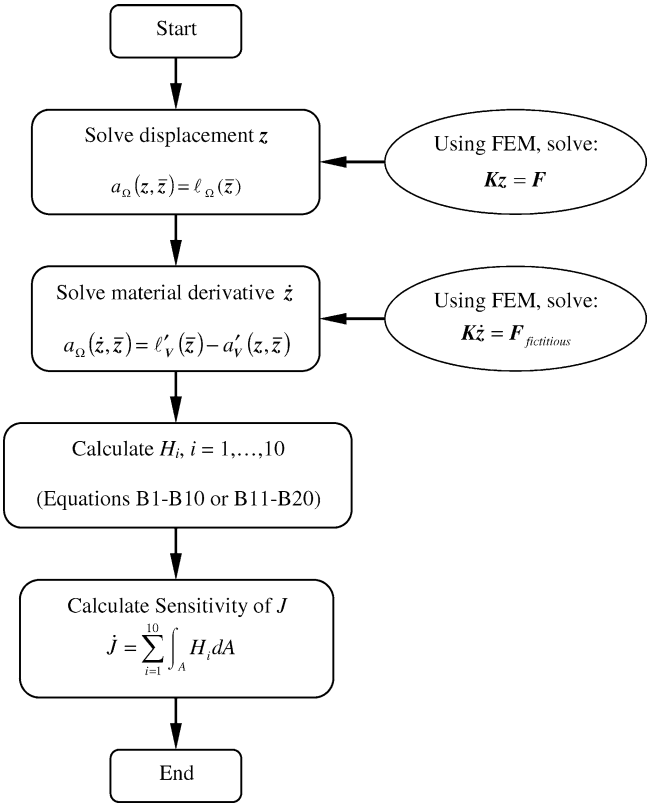

Fig. 3 A flowchart for continuum sensitivity analysis of crack size

and plane strain conditions, respectively. When inserted into Eq. (27), these expressions yield the first-order sensitivity of J with respect to crack size. Note that when the velocity field is unity at the crack tip, $\dot{J}$ is equal to $\partial J/\partial a$.

The integral in Eq. (27) is independent of the domain size A and can be calculated numerically using standard Gaussian quadrature. A 2×2 or higher integration rule is recommended to calculate $\dot{J}$. A flow diagram for calculating the sensitivity of J is shown in Fig. 3.

3.3 Velocity Field Definition

Defining the velocity field is an important step in continuum shape sensitivity analysis. Applying an inappropriate velocity field may yield inaccurate sensitivity results. The velocity field must meet several stringent theoretical and practical criteria [26]. A number of methods have been proposed in the literature to compute the velocity field [26]. The following example illustrates the one adopted in this study for sensitivity analysis of a mode-I fracture in FGM.

Consider an edge-cracked plate with length $2L$, width W and crack length a. Due to symmetry of the geometry only half of the plate has been modeled, as shown in Fig. 4. In Fig. 4, $ABCD$ is the domain of size $2b_1 \times b_2$ over which the J-integral and its sensitivity is evaluated, $\bar{L}$ is equal to half the length of plate (L) minus the maximum length of the finite element along the natural boundary in the x_2 direction. The velocity field $\boldsymbol{V}$ used in this study is defined as

$$\boldsymbol{V}(\boldsymbol{x}) = \begin{Bmatrix} V_1(\boldsymbol{x}) \\ V_2(\boldsymbol{x}) \end{Bmatrix} = V_{1,tip} \begin{Bmatrix} C_1(x_1)C_2(x_2) \\ 0 \end{Bmatrix}, \tag{41}$$

where

$$C_1(x_1) = \begin{cases} 1, & \text{if } |x_1| \le b_1 \\ \frac{x_1 - W + a}{b_1 - W + a}, & \text{if } x_1 > b_1 \\ \frac{x_1 + a}{a - b_1}, & \text{if } x_1 < -b_1 \end{cases}, \tag{42}$$

$$C_2(x_2) = \begin{cases} 1, & \text{if } x_2 \le b_2 \\ \frac{\bar{L} - x_2}{\bar{L} - b_2}, & \text{if } b_2 < x_2 \le \bar{L} \\ 0, & \text{if } x_2 > \bar{L} \end{cases}, \tag{43}$$

and $V_{1,tip} = V_1(\boldsymbol{0})$ is the x_1-component of velocity at the crack tip. Eq. (41) has been employed in all numerical examples presented in the next section. This velocity field ensures that the finite element mesh in the domain over which the J-integral and its sensitivity is evaluated have a virtual rigid body translation along with the

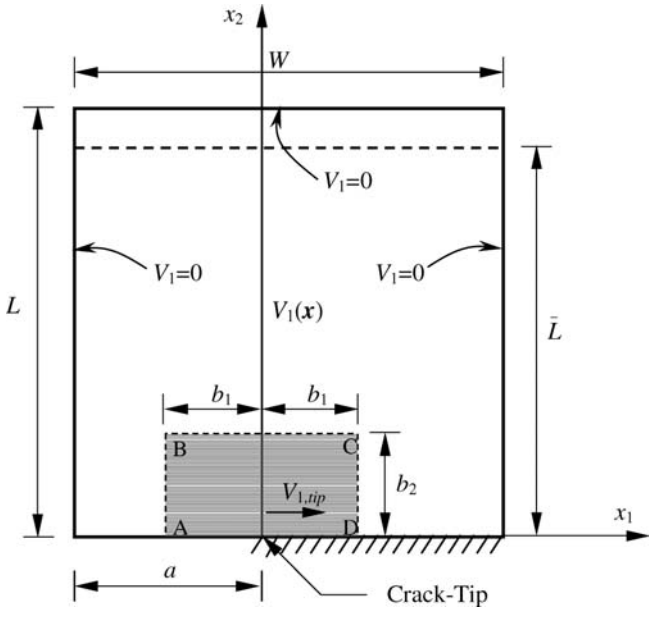

Fig. 4 Schematic for velocity field definition for cracked plate

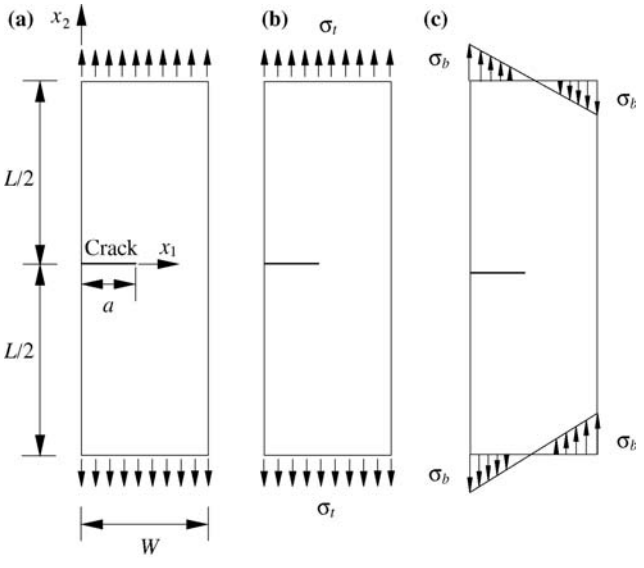

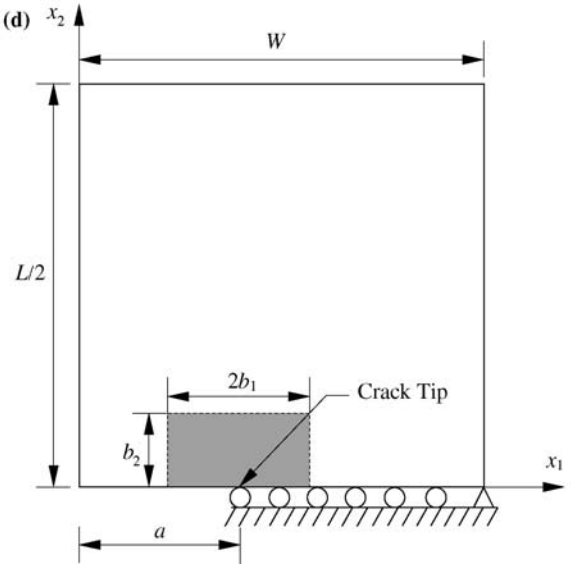

Fig. 5 Edge-cracked plate under mode I loading; **a** Geometry and loads for fixed grip loading; **b** Membrane loading; **c** Bending; and **d** Half model

crack tip. The velocity field is constant in the region $ABCD$, varies bi-linearly in rest of the domain, is zero along the boundary excluding the crack face and essential boundary, and varies linearly along the crack face and essential boundary.

4. Numerical examples

4.1 Example 1: Sensitivity Analysis of Edge-Cracked Plate

Consider an edge-cracked plate with length $L = 8$ units, width $W = 1$ unit, and crack length a, as shown in Fig. 5(a). Three loading conditions were considered, including uniform fixed grip loading (constant strain ε_0), membrane loading (constant tensile stress σ_t), and pure bending (linear stress σ_b). Figs. 5a, 5b, and 5c show the schematics of the three loading conditions. The elastic modulus was assumed to follow an exponential function, given by

$$E(x_1) = E_1 \exp(\eta x_1), 0 \le x_1 \le W, \tag{44}$$

where $E_1 = E(0)$, $E_2 = E(W)$, and $\eta = \ln(E_2/E_1)$. In Eq. (44), E_1 and η are two independent material parameters that characterize the elastic modulus variation. The following numerical values were used: $E_1 = 1$ unit, $E_2/E_1 = \exp(\eta) = 0.1, 0.2, 5,$ and 10, and $a/W = 0.1, 0.2, 0.3, 0.4, 0.5$ and 0.6 . Poisson's ratio was held constant with $v = 0.3$. A plane strain condition was assumed. Erdogan and Wu [27], who originally studied this example, provided a theoretical solution for normalized mode-I stress intensity factors.

Due to the symmetry of geometry and load, only half of the plate was analyzed, as shown in Fig. 5(d). FEM models used in the analysis for $a/W = 0.1, 0.2, 0.3, 0.4, 0.5$ and 0.6 are shown in Figs. 6 (a–f), respectively. FEM discretization for $a/W = 0.1$ involves 1421 nodes, 434 eight-noded quadrilateral elements, six focused quarter-point six-noded triangular elements, for $a/W = 0.2$ involves 1193 nodes, 360 eight-noded quadrilateral elements, six focused quarter-point six-noded triangular elements, for $a/W = 0.3$ involves 1205 nodes, 364 eight-noded quadrilateral elements, eight focused quarter-point six-noded triangular elements, for $a/W = 0.4$ involves 1289 nodes, 390 eight-noded quadrilateral elements, 12 focused quarter-point six-noded triangular elements, for $a/W = 0.5$ involves 1361 nodes, 412 eight-noded quadrilateral elements, 16 focused quarter-point six-noded triangular elements and for $a/W = 0.6$ involves 1289 nodes, 390 eight-noded quadrilateral elements, 12 focused quarter-point six-noded triangular elements. Depending on the a/W ratio, between six and 12 focused, quarter-point triangular elements were deployed to represent crack-tip singularity. A 2×2 Gaussian integration was employed. The size of the domain ($2b_1 \times b_2$) around the crack tip used to evaluate the J-integral and its sensitivity for $a/W = 0.1, 0.2, 0.3, 0.4, 0.5$ and 0.6 are respectively as

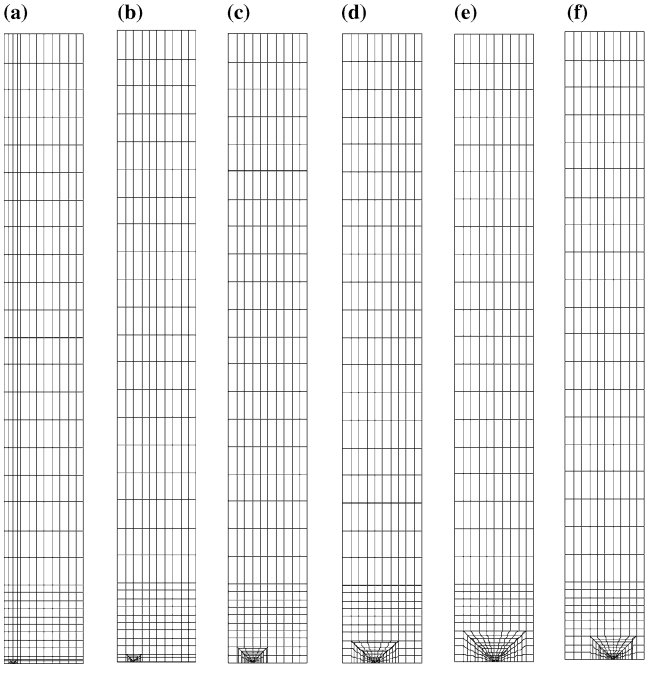

Fig. 6 FEM discretization of edge-cracked plate under mode I loading; **a** $a/W = 0.1$; **b** $a/W = 0.2$; **c** $a/W = 0.3$; **d** $a/W = 0.4$; (e) $a/W = 0.5$; and **f** $a/W = 0.6$

Table 1 Sensitivity of J for an edge-cracked plate by the proposed and finite-difference methods ($E_2/E_1 = 0.1$)

a/W	Normalized SIF[a]		Sensitivity of J-integral ($\partial J/\partial a$)		
	Present Results	Erodogan & Wu [27]	Proposed Method	Finite Difference	Difference[b] (percent)
a Fixed grip loading (constant strain ε_0)					
0.1	1.1577	1.1648	8.0745	8.0745	0.0002
0.2	1.2892	1.2963	18.0526	18.0527	0.0006
0.3	1.4965	1.5083	41.5662	41.5667	0.0012
0.4	1.8009	1.8246	99.9351	99.9367	0.0016
0.5	2.2583	2.3140	259.7135	259.7208	0.0028
0.6	2.9997	3.1544	772.5495	772.5706	0.0027
b Membrane loading (constant tensile stress σ_t)					
0.1	0.8096	0.8129	5.4641	5.4648	0.0120
0.2	1.2925	1.2965	23.0400	23.0408	0.0038
0.3	1.8488	1.8581	71.7504	71.7516	0.0017
0.4	2.5454	2.5699	206.2253	206.2301	0.0023
0.5	3.5001	3.5701	601.9136	601.9302	0.0028
0.6	4.9645	5.1880	1939.6908	1939.7545	0.0033
c Pure bending (linear stress σ_b)					
0.1	2.0289	2.0427	15.3509	15.3494	−0.0096
0.2	1.8907	1.9040	21.1042	21.1033	−0.0039
0.3	1.8662	1.8859	35.2488	35.2489	0.0005
0.4	1.9437	1.9778	66.9626	66.9627	0.0001
0.5	2.1468	2.2151	145.0595	145.0640	0.0031
0.6	2.5544	2.7170	373.0417	373.0470	0.0014

[a] Normalized SIF = $K_I/\sigma_0\sqrt{\pi a}$, $K_I/\sigma_t\sqrt{\pi a}$, $K_I/\sigma_b\sqrt{\pi a}$ for fixed grip, membrane, and pure bending loads, respectively

[b] Difference = ($\partial J/\partial a$ by finite-difference method – $\partial J/\partial a$ by proposed method) × $\partial J/\partial a$ 100 by finite-difference method

Table 2 Sensitivity of J for an edge-cracked plate by the proposed and finite-difference methods ($E_2/E_1 = 0.2$)

a/W	Normalized SIF[a]		Sensitivity of J-integral ($\partial J/\partial a$)		
	Present Results	Erodogan & Wu [27]	Proposed Method	Finite Difference	Difference[b] (percent)
a Fixed grip loading (constant strain ε_0)					
0.1	1.1627	1.1670	7.2425	7.2425	0.0003
0.2	1.3020	1.3058	15.1677	15.1678	0.0008
0.3	1.5269	1.5330	33.3988	33.3993	0.0014
0.4	1.8636	1.8751	77.6551	77.6564	0.0017
0.5	2.3775	2.4031	196.5079	196.5134	0.0028
0.6	3.2208	3.2981	571.9119	571.9329	0.0037
b Membrane loading (constant tensile stress σ_t)					
0.1	1.0519	1.0553	6.2970	6.2969	−0.0007
0.2	1.3925	1.3956	18.5807	18.5809	0.0010
0.3	1.8338	1.8395	48.9682	48.9688	0.0012
0.4	2.4314	2.4436	127.5675	127.5700	0.0020
0.5	3.2959	3.3266	348.8805	348.8897	0.0026
0.6	4.6717	4.7614	1073.4914	1073.5312	0.0037
c Pure bending (linear stress σ_b)					
0.1	1.6675	1.6743	9.4842	9.4843	0.0017
0.2	1.5893	1.5952	12.4843	12.4843	0.0003
0.3	1.6037	1.6122	20.2284	20.2288	0.0020
0.4	1.7070	1.7210	37.4875	37.4879	0.0011
0.5	1.9264	1.9534	79.4636	79.4662	0.0033
0.6	2.3419	2.4037	200.3289	200.3363	0.0037

[a] Normalized SIF = $K_I/\sigma_0\sqrt{\pi a}$, $K_I/\sigma_t\sqrt{\pi a}$, $K_I/\sigma_b\sqrt{\pi a}$ for fixed grip, membrane, and pure bending loads, respectively

[b] Difference = ($\partial J/\partial a$ by finite-difference method – $\partial J/\partial a$ by proposed method) × $\partial J/\partial a$ 100 by finite-difference method

Table 3 Sensitivity of J for an edge-cracked plate by the proposed and finite-difference methods ($E_2/E_1 = 5.0$)

a/W	Normalized SIF[a]		Sensitivity of J-integral ($\partial J/\partial a$)		
	Present Results	Erodogan & Wu [27]	Proposed Method	Finite Difference	Difference[b] (percent)
a Fixed grip loading (constant strain ε_0)					
0.1	1.2407	1.2372	4.9757	4.9757	0.0001
0.2	1.4965	1.4946	8.7112	8.7112	0.0005
0.3	1.9133	1.9118	16.7389	16.7391	0.0011
0.4	2.5748	2.5730	35.3423	35.3429	0.0016
0.5	3.6601	3.6573	83.2082	83.2101	0.0023
0.6	5.5760	5.5704	229.0280	229.0357	0.0034
b Membrane loading (constant tensile stress σ_t)					
0.1	0.9937	0.9908	2.4673	2.4673	0.0002
0.2	1.1334	1.1318	3.5414	3.5414	−0.0004
0.3	1.3709	1.3697	6.0340	6.0341	0.0013
0.4	1.7498	1.7483	11.6301	11.6303	0.0016
0.5	2.3678	2.3656	25.4610	25.4615	0.0021
0.6	3.4494	3.4454	66.0007	66.0028	0.0032
c Pure bending (linear stress σ_b)					
0.1	0.6405	0.6385	0.9514	0.9514	0.0002
0.2	0.6882	0.6871	1.0564	1.0564	−0.0019
0.3	0.7787	0.7778	1.4992	1.4992	0.0017
0.4	0.9246	0.9236	2.4829	2.4830	0.0016
0.5	1.1595	1.1518	4.7736	4.7737	0.0018
0.6	1.5620	1.5597	11.0239	11.0242	0.0029

[a] Normalized SIF = $K_I/\sigma_0\sqrt{\pi a}$, $K_I/\sigma_t\sqrt{\pi a}$, $K_I/\sigma_b\sqrt{\pi a}$ for fixed grip, membrane, and pure bending loads, respectively

[b] Difference = ($\partial J/\partial a$ by finite-difference method – $\partial J/\partial a$ by proposed method) × 100 by finite-difference method

Table 4 Sensitivity of J for an edge-cracked plate by the proposed and finite-difference methods ($E_2/E_1 = 10.0$)

a/W	Normalized SIF[a]		Sensitivity of J-integral ($\partial J/\partial a$)		
	Present Results	Erodogan & Wu [27]	Proposed Method	Finite Difference	Difference[b] (percent)
a Fixed grip loading (constant strain ε_0)					
0.1	1.2711	1.2664	4.7261	4.7261	0.0001
0.2	1.5762	1.5740	8.2725	8.2725	0.0006
0.3	2.0739	2.0723	15.7277	15.7279	0.0011
0.4	2.8752	2.8736	33.0064	33.0069	0.0015
0.5	4.2159	4.2140	77.4798	77.4817	0.0024
0.6	6.6340	6.6319	213.0891	213.0965	0.0035
b Membrane loading (constant tensile stress σ_t)					
0.1	0.8664	0.8631	1.6960	1.6960	−0.0015
0.2	1.0035	1.0019	2.2681	2.2681	0.0001
0.3	1.2302	1.2291	3.6603	3.6604	0.0015
0.4	1.5896	1.5884	6.7545	6.7546	0.0007
0.5	2.1775	2.1762	14.2718	14.2722	0.0027
0.6	3.2138	3.2124	35.9205	35.9217	0.0035
c Pure bending (linear stress σ_b)					
0.1	0.5102	0.5082	0.5625	0.5625	−0.0026
0.2	0.5658	0.5648	0.6124	0.6124	−0.0003
0.3	0.6595	0.6588	0.8508	0.8508	0.0021
0.4	0.8050	0.8043	1.3787	1.3787	−0.0004
0.5	1.0358	1.0350	2.5977	2.5978	0.0031
0.6	1.4294	1.4286	5.8906	5.8908	0.0037

[a] Normalized SIF = $K_I/\sigma_0\sqrt{\pi a}$, $K_I/\sigma_t\sqrt{\pi a}$, $K_I/\sigma_b\sqrt{\pi a}$ for fixed grip, membrane, and pure bending loads, respectively

[b] Difference = ($\partial J/\partial a$ by finite-difference method – $\partial J/\partial a$ by proposed method) × $\partial J/\partial a$ 100 by finite-difference method

follows: 0.1 × 0.05, 0.2 × 0.1, 0.4 × 0.2, 0.6 × 0.3, 0.8 × 0.4, and 0.6 × 0.3 units.

Table 1 shows normalized mode-I stress intensity factors $K_I/\sigma_0\sqrt{\pi a}$, $K_I/\sigma_t\sqrt{\pi a}$, $K_I/\sigma_b\sqrt{\pi a}$, and $\partial J/\partial a$ under fixed grip, membrane loading, and bending, respectively for various a/W ratios and for $E_2/E_1 = 0.1$, where $\sigma_0 = E_1\varepsilon_0/(1-\nu^2)$, $\varepsilon_0 = 1$, $\sigma_t = \sigma_b = 1$ unit. Results show that the predicted, normalized SIF obtained in the present study agrees very well with the analytical results of Erdogan and Wu [27] for all three types of loading and for various a/W ratios. Table 1 also presents the numerical results of $\partial J/\partial a$. Two sets of results are shown for $\partial J/\partial a$, the first computed using the proposed method and the second calculated using the finite-difference method. A perturbation of 10^{-5} times the crack length was used in the finite-difference calculations. The results in Table 1 demonstrate that continuum shape sensitivity analysis provides accurate estimates of $\partial J/\partial a$ when compared with corresponding results using the finite-difference method. Unlike the virtual crack extension technique, no mesh perturbation is required using the proposed method. Similar results are presented in Table 2 for $E_2/E_1 = 0.2$, in Table 3 for $E_2/E_1 = 5.0$, and in Table 4 for $E_2/E_1 = 10.0$. The results in Tables 1–4 demonstrate that continuum shape sensitivity analysis provides accurate estimates of $\partial J/\partial a$ for various combinations of loading conditions, a/W, and E_2/E_1 ratios. The maximum difference between the

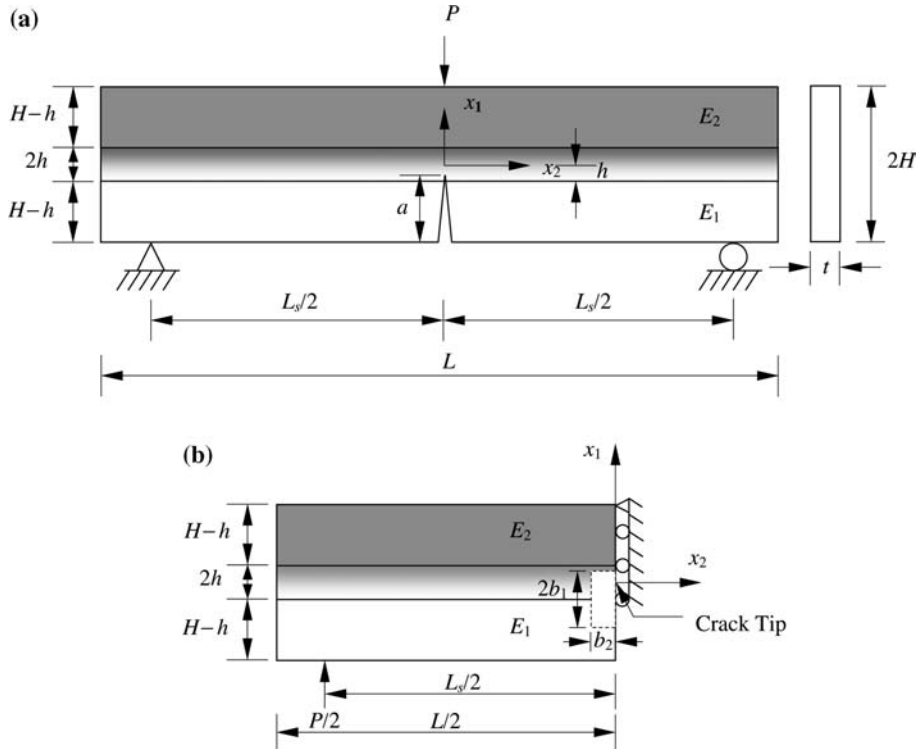

Fig. 7 Three-point bend specimen under mode I loading; **a** Geometry and loads; and **b** Half model

results of proposed and finite-difference methods is less than 0.012 percent.

4.2 Example 2: Sensitivity Analysis of Three-Point Bend Specimen under Mode-I

Consider a three-point bend specimen with length $L = 54$ units, depth $2H = 10$ units, and thickness $t = 1$ unit, as shown in Fig. 7(a). A concentrated load $P = 1$ unit was applied at the middle of the beam of span $L_S = 50$ units and two supports were symmetrically placed with respect to an edge crack of length a. In the depth direction, the beam consists of $2h$ units deep FGM sandwiched between two distinct homogeneous materials, each of which has a depth of $H - h$. E_1 and E_2 represent the elastic moduli of the bottom and top layers. Two types of elastic modulus variations were considered: linear variation and exponential variation of the FGM layer, with the end values matching the properties of the bottom and top layers. Mathematically, linear variation is defined as

$$E(x_1) = \begin{cases} E_2, & x_1 \geq h \\ \frac{E_1+E_2}{2} + \frac{E_2-E_1}{2h}x_1, & -h \leq x_1 \leq h \\ E_1, & x_1 \leq -h \end{cases} \tag{45}$$

and exponential variation is defined as

$$E(x_1) = \begin{cases} E_2, & x_1 \geq h \\ \sqrt{E_1 E_2}\exp\left(\frac{x_1}{2h}\ln\frac{E_2}{E_1}\right), & -h \leq x_1 \leq h \\ E_1, & x_1 \leq -h \end{cases}, \tag{46}$$

where E_1, E_2, and $2h$ are material parameters. The following numerical values were chosen: $2h = 1$ unit, $E_1 = 1$ unit, and $E_2/E_1 = 0.05, 0.1, 0.2, 0.5, 1, 2, 5, 10,$ and 20. For each E_2/E_1 ratio, three different crack lengths with $a/2H = 0.45, 0.5$ and 0.55 were selected with crack tips either at the middle of the FGM layer $(a/2H = 0.5)$, or at the material interfaces

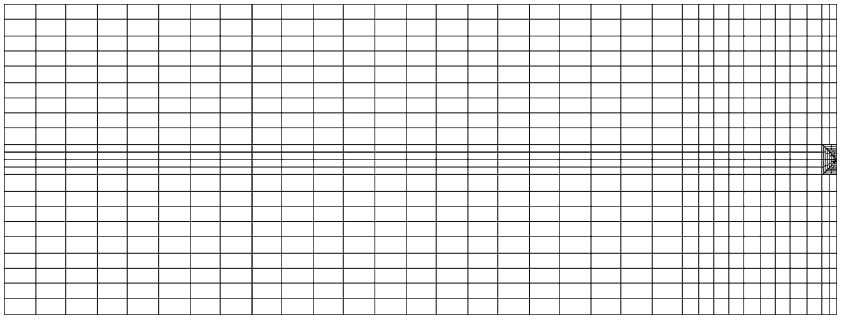

Fig. 8 FEM discretization of three-point bend specimen with a/2H = 0.50 under mode I loading

($a/2H = 0.45$ or 0.55). Poisson's ratio was held constant at $\nu = 0.3$. A plane stress condition was assumed.

Due to symmetric geometry and loading with respect to the crack, only a half model of the beam was analyzed, as shown in Fig. 7(b). FEM discretization of the half beam model for $a/2H = 0.45, 0.5$ and 0.55 involves 2669 nodes, 838 eight-noded quadrilateral elements, eight focused quarter-point six-noded triangular elements. Typical FEM discretization for $a/2H = 0.5$ is shown in Figs. 8. A 2×2 Gaussian integration was employed. A domain size of 8×5 units around the crack tip was used to evaluate the J-integral and its sensitivity.

Table 5 shows the predicted normalized mode-I SIF $K_I\sqrt{H}/P$, obtained in the present study for $a/2H = 0.45$ and various combinations of E_2/E_1, as well as for linear and exponential variations of the elastic modulus. Table 5 also presents the numerical results of $\partial J/\partial a$ for both linear and exponential elastic modulus variations. Two sets of results are shown for $\partial J/\partial a$, the first computed using the proposed method and second calculated using the finite-difference method. A perturbation of 10^{-5} times the crack length was used for finite-difference calculations. The results in Table 5 demonstrate that continuum shape sensitivity analysis again provides accurate estimates of $\partial J/\partial a$ as compared with corresponding results from the finite-difference method for various E_2/E_1 under both linear and exponential elastic modulus variations. Similar results are presented in Table 6 for $a/2H = 0.50$, and in Table 7 for $a/2H = 0.55$. Indeed, the results in Tables 5–7 demonstrate that continuum shape sensitivity analysis provides accurate estimates of $\partial J/\partial a$ for various combinations of elastic modulus variations, E_2/E_1, and $a/2H$ ratios.

Table 5 Sensitivity of J for three-point bend specimen by the proposed and finite-difference methods ($a/2H = 0.45$)

E_2/E_1	Present Results ($K_I\sqrt{H}/P$)	Sensitivity of J-integral ($\partial J/\partial a$)		
		Proposed Method	Finite Difference	Difference[a] (percent)
a Linear Variation				
0.05	32.4069	467.7523	467.7689	0.0035
0.1	23.3146	198.2592	198.2623	0.0016
0.2	17.3461	80.2695	80.2709	0.0017
0.5	11.6568	22.4226	22.4227	0.0004
1	8.1420	7.7004	7.7004	0.0009
2	5.2322	4.3617	4.3617	0.0004
5	2.5268	5.1632	5.1631	−0.0011
10	1.3240	4.9711	4.9709	−0.0027
20	0.6735	3.5769	3.5767	−0.0054
b Exponential Variation				
0.05	31.6868	144.2164	144.2212	0.0033
0.1	23.0812	77.7745	77.7763	0.0023
0.2	16.9573	40.1238	40.1240	0.0005
0.5	11.2333	15.8866	15.8869	0.0017
1	8.1420	7.7004	7.7004	0.0009
2	5.8630	3.6311	3.6311	0.0002
5	3.8133	1.1306	1.1306	−0.0008
10	2.7871	0.2980	0.2980	−0.0003
20	2.0593	−0.0417	−0.0417	0.0179

[a] Difference = ($\partial J/\partial a$ by finite-difference method − $\partial J/\partial a$ by proposed method) × $\partial J/\partial a$ 100 by finite-difference method

Table 6 Sensitivity of J for three-point bend specimen by the proposed and finite-difference methods ($a/2H = 0.50$)

E_2/E_1	Present Results ($K_I\sqrt{H}/P$)	Sensitivity of J-integral ($\partial J/\partial a$)		
		Proposed Method	Finite Difference	Difference[a] (percent)
a Linear Variation				
0.05	31.1898	1411.8779	1411.9621	0.0060
0.1	23.9149	555.1371	555.1524	0.0027
0.2	18.3227	204.2048	204.2077	0.0014
0.5	12.5795	40.8503	40.8507	0.0009
1	9.4678	11.2628	11.2628	0.0006
2	7.3161	5.2616	5.2616	−0.0001
5	5.4968	4.4094	4.4093	−0.0008
10	4.6112	3.8706	3.8705	−0.0026
20	4.0328	2.6829	2.6828	−0.0055
b Exponential Variation				
0.05	20.2541	369.3652	369.3809	0.0042
0.1	17.2310	169.3468	169.3481	0.0008
0.2	14.5336	75.7558	75.7565	0.0009
0.5	11.4374	25.7051	25.7053	0.0008
1	9.4678	11.2628	11.2628	0.0006
2	7.8416	4.8227	4.8227	0.0007
5	6.2115	1.3712	1.3712	0.0013
10	5.3110	0.3780	0.3780	0.0017
20	4.6126	−0.0024	−0.0024	−0.0987

[a] Difference = ($\partial J/\partial a$ by finite-difference method − $\partial J/\partial a$ by proposed method) × $\partial J/\partial a$ 100 by finite-difference method

Table 7 Sensitivity of J for three-point bend specimen by the proposed and finite-difference methods ($a/2H = 0.55$)

E_2/E_1	Present Results ($K_I\sqrt{H}/P$)	Sensitivity of J-integral ($\partial J/\partial a$)		
		Proposed Method	Finite Difference	Difference[a] (percent)
a Linear Variation				
0.05	15.2836	6695.6345	6696.1466	0.0076
0.1	13.8754	1366.1375	1366.1836	0.0034
0.2	12.8026	295.3975	295.4016	0.0014
0.5	11.7664	49.5108	49.5113	0.0008
1	11.1611	17.2040	17.2042	0.0011
2	10.6297	8.3144	8.3144	0.0009
5	9.9848	4.9074	4.9074	−0.0004
10	9.5873	3.3001	3.3000	−0.0014
20	9.3017	1.7388	1.7388	−0.0020
b Exponential Variation				
0.05	11.5808	437.5786	437.5634	−0.0035
0.1	11.4819	208.7195	208.7213	0.0008
0.2	11.3826	99.0466	99.0452	−0.0014
0.5	11.2539	36.6429	36.6432	0.0008
1	11.1611	17.2040	17.2042	0.0011
2	11.0802	8.0782	8.0782	0.0004
5	11.0212	2.9177	2.9177	0.0004
10	11.0423	1.2681	1.2681	0.0002
20	11.1399	0.4919	0.4919	0.0001

[a] Difference = ($\partial J/\partial a$ by finite-difference method − $\partial J/\partial a$ by proposed method) × $\partial J/\partial a$ 100 by finite-difference method

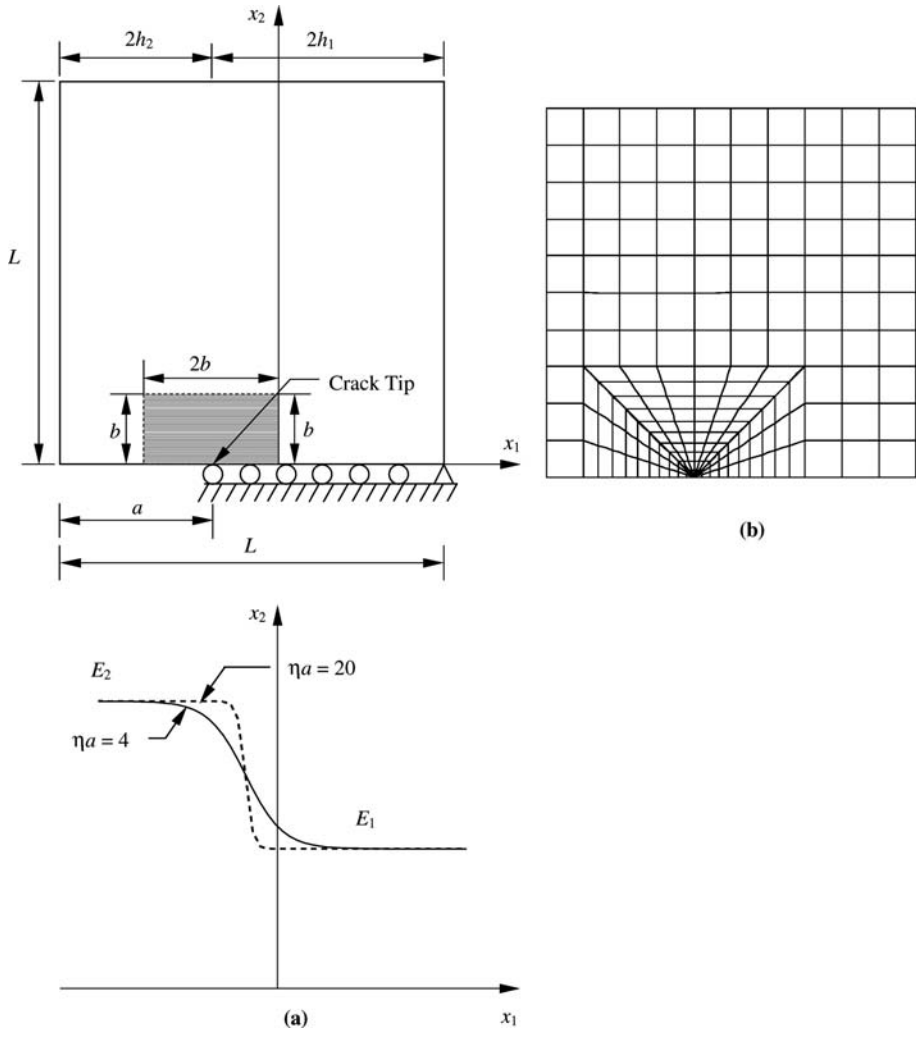

Fig. 9 Composite strip under mode-I loading; **a** Geometry and Elastic modulus variation; **b** FEM discretization (649 nodes, 190 8-noded quadrilateral elements, 12 focused quarter-point 6-noded triangular elements)

4.3 Example 3: Sensitivity Analysis of Composite Strip

In the final example, consider the square composite strip configuration studied by Eischen [28] with size $L = 1$ unit, $2h_1 = 0.6$ units and $2h_2 = 0.4$ units, as shown in Fig. 9(a). A crack of length $a = 0.4$ units is located on the line $x_2 = 0$. Poisson's ratio was held constant at $v = 0.3$. The elastic modulus was assumed to vary smoothly according to a hyperbolic-tangent function, given by

$$E(x_1) = \frac{E_1 + E_2}{2} + \frac{E_1 - E_2}{2} \tanh[\eta(x_1 + 0.1)], \quad -0.5 \le x_1 \le 0.5, \tag{47}$$

where E_1 and E_2 are the bounds of $E(x_1)$, and η is a non-homogeneity parameter that controls the variation of $E(x_1)$ from E_1 to E_2, as shown in Fig. 9(a). When $\eta \to \infty$, a sharp discontinuity occurs in the slope of $E(x_1)$ across the interface at $x_1 = -0.1$. A tensile load corresponding to $\sigma_{22}(x_1, 1) = \bar{\varepsilon}E(x_1)/(1 - v^2)$ was applied at the top edge, which results in a uniform strain $\varepsilon_{22}(x_1, x_2) = \bar{\varepsilon}$ in the corresponding uncracked structure. The following numerical values were used: $E_1 = 1$ unit, $E_2 = 3$ units, $\eta a = 0, 2, 4, 6,$ and 20 units, and $\bar{\varepsilon} = 1$. A plane strain condition was assumed.

The FEM discretization used in the analysis is shown in Figure 9(b). A 2×2 Gaussian integration was employed. A domain of size $2b_1 \times b_2$ with $b_1 = b_2 = 0.3$ units was used around the crack tip to evaluate the J-integral and its sensitivity.

Table 8 Sensitivity of J for a composite strip configuration by the proposed and finite-difference methods

ηa	$K_I/\bar{\varepsilon}\bar{E}(-0.5)\sqrt{\pi a}$		Sensitivity of J-integral ($\partial J/\partial a$)		
	Eischen [28]	Present Results	Proposed Method	Finite Difference	Difference[a] (percent)
0.0	2.112	2.1127	79.4463	79.4464	0.0002
2.0	2.295	2.2967	236.3875	236.3879	0.0002
4.0	2.571	2.5732	330.9231	330.9235	0.0001
6.0	2.733	2.7355	398.1568	398.1570	0.0001
20.0	3.228	3.2192	676.6920	676.6838	−0.0012

[a] Difference = ($\partial J/\partial a$ by finite-difference method − $\partial J/\partial a$ by proposed method) × $\partial J/\partial a$ 100 by finite-difference method

Table 8 compares the predicted normalized mode-I SIF $K_I/[\bar{\varepsilon}E(-0.5)\sqrt{\pi a}]$ obtained in the present study with Eischen's results [28] for several values of ηa. The normalized SIF results obtained in the present study agree very well with the reference solution. Table 8 also presents the numerical results of $\partial J/\partial a$ for several values of ηa. Two sets of results are shown for $\partial J/\partial a$, the first computed using the proposed method and second calculated using the finite-difference method. As before, a perturbation of 10^{-5} times the crack length was used for finite-difference calculations. Results in Table 8 demonstrate that continuum shape sensitivity analysis provides accurate estimates of $\partial J/\partial a$ as compared with corresponding results from the finite-difference method for various values of ηa. There were no discrepancies in results even when $\eta a = 20$, representing sharp discontinuity in the slope of $E(x_1)$ at $x_1 = -0.1$ [see Fig. 9(a)].

5. Summary and conclusions

A new method is presented for conducting continuum shape sensitivity analyses of a crack in isotropic, linear-elastic, functionally graded materials. This method involves the material derivative concept from continuum mechanics, domain integral representation of a J-integral or an interaction integral, and direct differentiation. Unlike virtual crack extension techniques, no mesh perturbation is needed in the proposed method to calculate the sensitivity of stress-intensity factors. Since the governing variational equation is differentiated prior to discretization, the resulting sensitivity equations are independent of approximate numerical techniques, such as the meshless method, finite element method, boundary element method, or others. Also, since the proposed method requires only the first-order sensitivity of a displacement field, it is much simpler and more efficient than existing methods. Numerical results show that first-order sensitivities of the J-integral obtained using the proposed method are in excellent agreement with the reference solutions obtained from finite-difference methods for the structural and crack geometries considered.

Acknowledgements

The authors would like to acknowledge the financial support of the U.S. National Science Foundation (NSF) under Award Nos. CMS-9733058 and CMS-0409463.

Appendix A. The h-functions

For plane stress,

$$h_1 = \frac{E\varepsilon_{11}^2}{2(1-\nu^2)}\frac{\partial q}{\partial x_1}, \tag{A1}$$

$$h_2 = \frac{E\varepsilon_{12}}{(1+\nu)}\frac{\partial z_2}{\partial x_2}\frac{\partial q}{\partial x_1}, \tag{A2}$$

$$h_3 = \frac{E\varepsilon_{11}\varepsilon_{12}}{(1+\nu)}\frac{\partial q}{\partial x_2}, \tag{A3}$$

$$h_4 = \frac{E(\varepsilon_{22}+\nu\varepsilon_{11})}{1-\nu^2}\frac{\partial z_2}{\partial x_1}\frac{\partial q}{\partial x_2}, \tag{A4}$$

$$h_5 = \frac{E\varepsilon_{22}^2}{2(1-\nu^2)}\frac{\partial q}{\partial x_1}, \tag{A5}$$

$$h_6 = \frac{E\varepsilon_{12}^2}{(1+\nu)}\frac{\partial q}{\partial x_1}, \tag{A6}$$

$$h_7 = \frac{\varepsilon_{11}^2 q}{2(1-\nu^2)}\frac{\partial E}{\partial x_1}, \tag{A7}$$

$$h_8 = \frac{\nu\varepsilon_{11}\varepsilon_{22}q}{1-\nu^2}\frac{\partial E}{\partial x_1}, \tag{A8}$$

$$h_9 = \frac{\varepsilon_{22}^2 q}{2(1-\nu^2)}\frac{\partial E}{\partial x_1} \tag{A9}$$

and

$$h_{10} = \frac{\varepsilon_{12}^2 q}{(1+\nu)}\frac{\partial E}{\partial x_1}. \tag{A10}$$

For plane strain,

$$h_1 = \frac{(1-\nu)E\varepsilon_{11}^2}{2(1+\nu)(1-2\nu)}\frac{\partial q}{\partial x_1}, \tag{A11}$$

$$h_2 = \frac{E\varepsilon_{12}}{(1+\nu)}\frac{\partial z_2}{\partial x_1}\frac{\partial q}{\partial x_1}, \tag{A12}$$

$$h_3 = \frac{E\varepsilon_{11}\varepsilon_{12}}{(1+\nu)}\frac{\partial q}{\partial x_2}, \tag{A13}$$

$$h_4 = \frac{E((1-\nu)\varepsilon_{22}+\nu\varepsilon_{11})}{(1+\nu)(1-2\nu)}\frac{\partial z_2}{\partial x_1}\frac{\partial q}{\partial x_2}, \tag{A14}$$

$$h_5 = \frac{(1-\nu)E\varepsilon_{22}^2}{2(1+\nu)(1-2\nu)}\frac{\partial q}{\partial x_1}, \tag{A15}$$

$$h_6 = \frac{E\varepsilon_{12}^2}{(1+\nu)}\frac{\partial q}{\partial x_1}, \tag{A16}$$

$$h_7 = \frac{(1-\nu)\varepsilon_{11}^2 q}{2(1+\nu)(1-2\nu)}\frac{\partial E}{\partial x_1}, \tag{A17}$$

$$h_8 = \frac{\nu\varepsilon_{11}\varepsilon_{22}q}{(1+\nu)(1-2\nu)}\frac{\partial E}{\partial x_1}, \tag{A18}$$

$$h_9 = \frac{(1-\nu)\varepsilon_{22}^2 q}{2(1+\nu)(1-2\nu)}\frac{\partial E}{\partial x_1} \tag{A19}$$

and

$$h_{10} = \frac{\varepsilon_{12}^2 q}{(1+\nu)}\frac{\partial E}{\partial x_1}. \tag{A20}$$

In Equations A1–A20, $E = E(x_1)$ and v = constant. When E = constant, h_7–h_{10} vanish, as expected and h_1–h_6 degenerate to corresponding equations for homogeneous materials [19].

Appendix B. The H-functions

For plane stress,

$$H_1 = \frac{E\varepsilon_{11}}{(1-v^2)}\frac{\partial \dot{z}_1}{\partial x_1}\frac{\partial q}{\partial x_1} + \frac{\varepsilon_{11}^2 V_1}{2(1-v^2)}\frac{\partial E}{\partial x_1}\frac{\partial q}{\partial x_1}, \tag{B1}$$

$$H_2 = \frac{E}{2(1+v)}\left(\frac{\partial \dot{z}_1}{\partial x_2} + \frac{\partial \dot{z}_2}{\partial x_1}\right)\frac{\partial z_2}{\partial x_1}\frac{\partial q}{\partial x_1} + \frac{E\varepsilon_{12}}{(1+v)}\frac{\partial \dot{z}_2}{\partial x_1}\frac{\partial q}{\partial x_1} + \frac{\varepsilon_{12}V_1}{(1+v)}\frac{\partial E}{\partial x_1}\frac{\partial z_2}{\partial x_1}\frac{\partial q}{\partial x_1}, \tag{B2}$$

$$H_3 = \frac{E\varepsilon_{11}}{2(1+v)}\left(\frac{\partial \dot{z}_1}{\partial x_2} + \frac{\partial \dot{z}_2}{\partial x_1}\right)\frac{\partial q}{\partial x_2} + \frac{E\varepsilon_{12}}{(1+v)}\frac{\partial \dot{z}_1}{\partial x_1}\frac{\partial q}{\partial x_2} + \frac{\varepsilon_{11}\varepsilon_{12}V_1}{(1+v)}\frac{\partial E}{\partial x_1}\frac{\partial q}{\partial x_2}, \tag{B3}$$

$$H_4 = \frac{E}{1-v^2}\frac{\partial \dot{z}_2}{\partial x_2}\frac{\partial z_2}{\partial x_1}\frac{\partial q}{\partial x_2} + \frac{vE}{1-v^2}\frac{\partial \dot{z}_1}{\partial x_1}\frac{\partial z_2}{\partial x_1}\frac{\partial q}{\partial x_2} + \frac{E\varepsilon_{22}}{1-v^2}\frac{\partial \dot{z}_2}{\partial x_1}\frac{\partial q}{\partial x_2} + \frac{vE\varepsilon_{11}}{1-v^2}\frac{\partial \dot{z}_2}{\partial x_1}\frac{\partial q}{\partial x_2} + \frac{\varepsilon_{22}V_1}{1-v^2}\frac{\partial E}{\partial x_1}\frac{\partial z_2}{\partial x_1}\frac{\partial q}{\partial x_2} + \frac{v\varepsilon_{11}V_1}{1-v^2}\frac{\partial E}{\partial x_1}\frac{\partial z_2}{\partial x_1}\frac{\partial q}{\partial x_2}, \tag{B4}$$

$$H_5 = \frac{E\varepsilon_{22}}{1-v^2}\frac{\partial \dot{z}_2}{\partial x_2}\frac{\partial q}{\partial x_1} + \frac{\varepsilon_{22}^2 V_1}{2(1-v^2)}\frac{\partial E}{\partial x_1}\frac{\partial q}{\partial x_1}, \tag{B6}$$

$$H_6 = \frac{E\varepsilon_{12}}{(1+v)}\left(\frac{\partial \dot{z}_1}{\partial x_2} + \frac{\partial \dot{z}_2}{\partial x_1}\right)\frac{\partial q}{\partial x_1} + \frac{\varepsilon_{12}^2 V_1}{(1+v)}\frac{\partial E}{\partial x_1}\frac{\partial q}{\partial x_1}, \tag{B5}$$

$$H_7 = \frac{\varepsilon_{11}q}{1-v^2}\frac{\partial \dot{z}_1}{\partial x_1}\frac{\partial E}{\partial x_1} + \frac{\varepsilon_{11}^2 q V_1}{2(1-v^2)}\frac{\partial^2 E}{\partial x_1^2}, \tag{B7}$$

$$H_8 = \frac{v\varepsilon_{22}q}{1-v^2}\frac{\partial \dot{z}_1}{\partial x_1}\frac{\partial E}{\partial x_1} + \frac{v\varepsilon_{11}q}{1-v^2}\frac{\partial \dot{z}_2}{\partial x_2}\frac{\partial E}{\partial x_1} + \frac{v\varepsilon_{11}\varepsilon_{22}qV_1}{1-v^2}\frac{\partial^2 E}{\partial x_1^2}, \tag{B8}$$

$$H_9 = \frac{\varepsilon_{22}q}{1-v^2}\frac{\partial \dot{z}_2}{\partial x_2}\frac{\partial E}{\partial x_1} + \frac{\varepsilon_{22}^2 qV_1}{2(1-v^2)}\frac{\partial^2 E}{\partial x_1^2} \tag{B9}$$

and

$$H_{10} = \frac{\varepsilon_{12}q}{(1+v)}\left(\frac{\partial \dot{z}_1}{\partial x_2} + \frac{\partial \dot{z}_2}{\partial x_1}\right)\frac{\partial E}{\partial x_1} + \frac{\varepsilon_{12}^2 qV_1}{(1+v)}\frac{\partial^2 E}{\partial x_1^2}. \tag{B10}$$

For plane strain,

$$H_1 = \frac{(1-v)E\varepsilon_{11}}{(1+v)(1-2v)}\frac{\partial \dot{z}_1}{\partial x_1}\frac{\partial q}{\partial x_1} + \frac{(1-v)\varepsilon_{11}^2 V_1}{2(1+v)(1-2v)}\frac{\partial E}{\partial x_1}\frac{\partial q}{\partial x_1}, \tag{B11}$$

$$H_2 = \frac{E}{2(1+v)}\left(\frac{\partial \dot{z}_1}{\partial x_2} + \frac{\partial \dot{z}_2}{\partial x_1}\right)\frac{\partial z_2}{\partial x_1}\frac{\partial q}{\partial x_1} + \frac{E\varepsilon_{12}}{(1+v)}\frac{\partial \dot{z}_2}{\partial x_1}\frac{\partial q}{\partial x_1} + \frac{\varepsilon_{12}V_1}{(1+v)}\frac{\partial E}{\partial x_1}\frac{\partial z_2}{\partial x_1}\frac{\partial q}{\partial x_1}, \tag{B12}$$

$$H_3 = \frac{E\varepsilon_{11}}{2(1+v)}\left(\frac{\partial \dot{z}_1}{\partial x_2} + \frac{\partial \dot{z}_2}{\partial x_1}\right)\frac{\partial q}{\partial x_2} + \frac{E\varepsilon_{12}}{(1+v)}\frac{\partial \dot{z}_1}{\partial x_1}\frac{\partial q}{\partial x_2} + \frac{\varepsilon_{11}\varepsilon_{12}V_1}{(1+v)}\frac{\partial E}{\partial x_1}\frac{\partial q}{\partial x_2}, \tag{B13}$$

$$H_4 = \frac{(1-v)E}{(1+v)(1-2v)}\frac{\partial \dot{z}_2}{\partial x_2}\frac{\partial z_2}{\partial x_1}\frac{\partial q}{\partial x_2} + \frac{vE}{(1+v)(1-2v)}\frac{\partial \dot{z}_1}{\partial x_1}\frac{\partial z_2}{\partial x_1}\frac{\partial q}{\partial x_2} + \frac{(1-v)E\varepsilon_{22}}{(1+v)(1-2v)}\frac{\partial \dot{z}_2}{\partial x_1}\frac{\partial q}{\partial x_2} + \frac{vE\varepsilon_{11}}{(1+v)(1-2v)}\frac{\partial \dot{z}_2}{\partial x_1}\frac{\partial q}{\partial x_2} + \frac{(1-v)\varepsilon_{22}V_1}{(1+v)(1-2v)}\frac{\partial E}{\partial x_1}\frac{\partial z_2}{\partial x_1}\frac{\partial q}{\partial x_2} + \frac{v\varepsilon_{11}V_1}{(1+v)(1-2v)}\frac{\partial E}{\partial x_1}\frac{\partial z_2}{\partial x_1}\frac{\partial q}{\partial x_2}, \tag{B14}$$

$$H_5 = \frac{(1-v)E\varepsilon_{22}}{(1+v)(1-2v)}\frac{\partial \dot{z}_2}{\partial x_2}\frac{\partial q}{\partial x_1} + \frac{(1-v)\varepsilon_{22}^2 V_1}{2(1+v)(1-2v)}\frac{\partial E}{\partial x_1}\frac{\partial q}{\partial x_1}, \tag{B15}$$

$$H_6 = \frac{E\varepsilon_{12}}{(1+v)}\left(\frac{\partial \dot{z}_1}{\partial x_2} + \frac{\partial \dot{z}_2}{\partial x_1}\right)\frac{\partial q}{\partial x_1} + \frac{\varepsilon_{12}^2 V_1}{(1+v)}\frac{\partial E}{\partial x_1}\frac{\partial q}{\partial x_1}, \tag{B16}$$

$$H_7 = \frac{(1-v)\varepsilon_{11}q}{(1+v)(1-2v)}\frac{\partial \dot{z}_1}{\partial x_1}\frac{\partial E}{\partial x_1} + \frac{(1-v)\varepsilon_{11}^2 qV_1}{2(1+v)(1-2v)}\frac{\partial^2 E}{\partial x_1^2}, \tag{B17}$$

$$H_8 = \frac{v\varepsilon_{22}q}{(1+v)(1-2v)}\frac{\partial \dot{z}_1}{\partial x_1}\frac{\partial E}{\partial x_1} + \frac{v\varepsilon_{11}q}{(1+v)(1-2v)}\frac{\partial \dot{z}_2}{\partial x_2}\frac{\partial E}{\partial x_1} + \frac{v\varepsilon_{11}\varepsilon_{22}qV_1}{(1+v)(1-2v)}\frac{\partial^2 E}{\partial x_1^2}, \tag{B18}$$

$$H_9 = \frac{(1-v)\varepsilon_{22}q}{(1+v)(1-2v)}\frac{\partial \dot{z}_2}{\partial x_2}\frac{\partial E}{\partial x_1} + \frac{(1-v)\varepsilon_{22}^2 qV_1}{2(1+v)(1-2v)}\frac{\partial^2 E}{\partial x_1^2} \tag{B19}$$

and

$$H_{10} = \frac{\varepsilon_{12} q}{(1+\nu)} \left(\frac{\partial \dot{z}_1}{\partial x_2} + \frac{\partial \dot{z}_2}{\partial x_1} \right) \frac{\partial E}{\partial x_1} + \frac{\varepsilon_{12}^2 q V_1}{(1+\nu)} \frac{\partial^2 E}{\partial x_1^2}. \quad \text{(B20)}$$

In Equations B1–B20, $E = E(x_1)$ and ν = constant. When E = constant, H_7–H_{10} vanish, as expected and H_1–H_6 degenerate to corresponding equations for homogeneous materials [19].

References

1. Suresh S, Mortensen A (1998) Fundamentals of functionally graded materials. IOM Communications Ltd., London
2. Erdogan F (1995) Fracture mechanics of functionally graded materials. Compo Eng 5(7) 753–770
3. Gu P, Dao M, Asaro RJ (1999) A simplified method for calculating the crack tip field of functionally graded materials using the domain integral. J Appl Mech 66:101–108
4. Rao BN, Rahman S (2003) Meshfree analysis of cracks in isotropic functionally graded materials Eng Frac Mech (2003) 70:1–27
5. Madsen HO, Krenk S, Lind NC (1986) Methods of Structural Safety, Prentice-Hall, Inc., Englewood Cliffs, New Jersey
6. Grigoriu M, Saif MTA, El-Borgi S, Ingraffea A (1990) Mixed-mode fracture initiation and trajectory prediction under random stresses. 45:19–34
7. Provan James W (1987) Probabilistic fracture mechanics and reliability, martinus nijhoff publishers, Dordrecht, The Netherlands
8. Besterfield GH, Liu WK, Lawrence MA, Belytschko T (1991) Fatigue crack growth reliability by probabilistic finite elements. Comput Methods Appl Mech Eng 86:297–320
9. Besterfield GH, Lawrence MA, Belytschko T (1990) Brittle fracture reliability by probabilistic finite elements. ASCE J Eng Mech 116(3):642–659
10. Rahman S (1995) A stochastic model for elastic-plastic fracture analysis of circumferential through-wall-cracked pipes subject to bending. Eng Fracture Mech 52(2):265–288
11. Rahman S, Kim J-S (2000) Probabilistic fracture mechanics for nonlinear structures. Int J Pre issue Vessels Piping 78(4):9–17
12. Rahman S (2001) Probabilistic fracture mechanics by J-estimation and finite element methods. 68:107–125
13. Lin SC, Abel J (1988) Variational approach for a new direct-integration form of the virtual crack extension method. Int J Fracture 38:217–235
14. deLorenzi HG (1982) On the energy release rate and the J-integral for 3-d crack configurations. Int J Fracture 19:183–193
15. deLorenzi HG (1985) Energy release rate calculations by the finite element method. 21:Eng Fracture Mech 21:129–143
16. Haber RB, Koh HM (1985) Explicit expressions for energy release rates using virtual crack extensions. Int J Numer Methods in Eng 21:301–315
17. Barbero EJ, Reddy JN (1990) The jacobian derivative method for three-dimensional fracture mechanics. Commun Appl Numer Methods 6:507–518
18. Hwang CG, Wawrzynek PA, Tayebi AK, Ingraffea AR (1998) On the virtual crack extension method for calculation of the rates of energy release rate. Eng Fracture Mech 59:521–542
19. Chen G, Rahman S, Park YH (2002) Shape sensitivity analysis of linear-elastic cracked structures. ASME J Pres Vessel Tech 124(4):476–482
20. Chen G, Rahman S, Park YH (2001) Shape sensitivity and reliability analyses of linear-elastic cracked structures. Int J Fracture 112(3):223–246
21. Chen G, Rahman S, Park YH (2001) Shape sensitivity analysis in mixed-mode fracture mechanics. Compu Mech 27(4):282–291
22. Choi KK, Haug EJ (1983) Shape design sensitivity analysis of elastic structures. J Struc Mech 11(2):231–269
23. Haug EJ, Choi KK, Komkov V (1986) Design sensitivity analysis of structural systems. Academic Press, New York
24. Rice JR (1968) A path independent integral and the approximate analysis of strain concentration by notches and cracks. J Appl Mech 35:379–386
25. Moran B, Shih F (1987) Crack tip and associated domain integrals from momentum and energy balance. Eng Fracture Mech 27:615–642
26. Choi KK, Chang KH (1994) A study of design velocity field computation for shape optimal design. Finite Elem Anal Des 15:317–341
27. Erdogan F, Wu BH (1997) The surface crack problem for a plate with functionally graded properties. J Appl Mech 64:449–456
28. Eischen JW (1987) Fracture of nonhomogeneous materials. J Fracture 34:3–22, 1987